

# NLO EW and QCD proton-proton cross section calculations with `mcsanc-v1.01`

Sergey G. Bondarenko<sup>a,b</sup>, Andrey A. Saponov<sup>a,\*</sup>

<sup>a</sup>*Dzhelepov Laboratory for Nuclear Problems, JINR, Joliot-Curie 6, RU-141980 Dubna, Russia*

<sup>b</sup>*Bogoliubov Laboratory of Theoretical Physics, JINR, Joliot-Curie 6, RU-141980 Dubna, Russia*

---

## Abstract

`mcsanc` is a Monte-Carlo tool based on the SANC (Support for Analytic and Numeric Calculations for experiments at colliders) modules for higher order calculations in hadron collider physics. It allows to evaluate NLO QCD and EW cross sections for Drell–Yan processes (inclusive), associated Higgs and gauge boson production and single-top quark production in s- and t-channel. The paper contains theoretical description of the SANC approach, numerical validations and manual.

**Keywords:** Perturbation theory; NLO calculations; Standard Model; Electroweak interaction; QCD; QED; Monte-Carlo integration;

---

## PROGRAM SUMMARY

*Program Title:* `mcsanc-v1.01`

*Journal Reference:*

*Catalogue identifier:*

*Licensing provisions:* none

*Programming language:* Fortran, C, C++

*Computer:* x86(-64) architecture

*Operating system:* Linux

*RAM:* 2 Gbytes

*Number of processors used:* multiprocess

*Classification:* 11.1, 11.6

*External routines/libraries:* LHAPDF [1]

*Subprograms used:* Looptools [2], Cuba [3]

*Nature of problem:* Theoretical calculations at next-to-leading order in perturbation theory allow to compute higher precision amplitudes for Standard Model processes and decays, provided proper treatments of UV divergences and IR singularities are performed.

*Solution method:* Numerical integration of the precomputed differential expressions for partonic cross sections of certain processes implemented as SANC modules [4].

*Restrictions:* the list of processes is limited to Drell–Yan, associated Higgs and gauge boson production and single-top production in s- and t-channel

*Running time:* from hours to days depending on requested precision and kinematic conditions

- [2] T. Hahn and M. Perez-Victoria, *Comput. Phys. Commun.* 118 (1999) 153–165, hep-ph/9807565
- [3] T. Hahn, *Comput. Phys. Commun.* 168 (2005) 78–95, hep-ph/0404043
- [4] A. Andonov, A. Arbuzov, D. Bardin, et al., *Comput. Phys. Commun.* 181 (2010) 305–312, arXiv:0812.4207

## 1. Introduction

Most demanded theoretical calculations for high energy particle interaction processes find their realization as a Monte-Carlo code usable by experimentalists. The Monte-Carlo tools can fulfill several tasks: calculate total and differential cross section or provide events in final state kinematics suitable for analysis simulation. For the first type we use here the term “integrator”. The second kind of tools is known as generators. Besides the calculation itself, such qualities as speed, functionality and configuration simplicity are valued.

The calculations of fully differential inclusive NNLO QCD cross section of the Drell–Yan (DY) processes are implemented in DYNLO [1, 2] and FEWZ [3] integrators. Recent FEWZ.v3.0 also includes electroweak NLO corrections. The DYRAD package provides NLO QCD calculations in the context of jets production on colliders utilizing the method of universal crossing functions [4]. The well known MCFM [5] package includes NLO QCD calculations for DY, associated Higgs and gauge boson production, single top quark production and large amount of other processes predicted for proton-(anti)proton collisions. There are number of codes that allow to compute complete  $\mathcal{O}(\alpha)$  corrections. There are WGRAD2 [6] and ZGRAD2 [7] for Drell–Yan charged and neutral currents respectively and the HORACE [8, 9] code for both neutral and charged currents. In this paper we describe a Monte-Carlo integrator `mcsanc-v1.01` [10] in which the processes

## References

- [1] M. R. Whalley, D. Bourilkov, and R. C. Group, hep-ph/0508110

---

\*Corresponding author.

E-mail address: andrey.a.saponov@gmail.com

of DY, Higgs-strahlung and single-top production in s- and t-channel are implemented with NLO QCD and EW corrections.

The paper is organized as follows. Section 2 contains details on next to leading order calculations in the SANC system, it describes treatment of singularities, electroweak scheme issues and code organization. Section 3 gives overview of numerical cross checks and validation performed for `mcsanc-v1.01` program and summary is given in Section 4. Appendix A contains technical information on the program's usage and configuration and Appendix B describes efficiency issues related to multiprocess runs.

## 2. NLO corrections in SANC package

The SANC system [11, 12] implements calculations of complete (real and virtual) NLO QCD and EW corrections for the Drell–Yan process, associative Higgs and gauge boson production, single top production and several other processes at partonic level. Here we give a brief summary of the main properties of this framework. For complete list of SANC processes see [12].

All calculations are performed within the OMS (on-mass-shell) renormalization scheme [13] in the  $R_\xi$  gauge which allows an explicit control of the gauge invariance by examining a cancellation of the gauge parameters in the analytical expression of the matrix element.

Depending on the process and type of corrections, we subdivide the total NLO cross section at the partonic level into several terms:

$$d\sigma = d\sigma^{\text{LO}} + d\sigma^{\text{virt}}(\lambda) + d\sigma^{\text{soft}}(\lambda, \bar{\omega}) + d\sigma^{\text{hard}}(\bar{\omega}), \quad (1)$$

differential over a generic observable which is a function of the final state momenta,  $\sigma^{\text{LO}}$  is the leading order cross section,  $\sigma^{\text{virt}}$  is a contribution of virtual (loop) corrections,  $\sigma^{\text{soft}}$  corresponds to a soft photon or gluon emission and  $\sigma^{\text{hard}}$  is a contribution of a hard (real) photon or gluon emission. The terms with auxiliary parameters  $\bar{\omega}$  (photon energy which separates phase spaces associated with the soft and hard photon emission) and  $\lambda$  (photon mass which regularizes infrared divergences) are introduced in the NLO EW calculations. They cancel out after summation and the differential NLO EW cross-section for infrared-safe observables does not depend on these parameters [14, 15, 16].

The list of processes implemented in the `mcsanc-v1.01` code is given in the Table 1 with the tree level diagrams shown in Figure 1.

Figures 2 and 3 show examples of diagrams of corresponding NLO EW and QCD contributions to the implemented processes.

Electroweak NLO radiative corrections contain terms proportional to logarithms of the quark masses,  $\ln(\hat{s}/m_{u,d}^2)$ . They come from the initial state radiation

pid	$f(p_1) + f(p_2) \rightarrow$	ref.
001	$e^+(p_3) + e^-(p_4)$	[17, 18]
002	$\mu^+(p_3) + \mu^-(p_4)$	
003	$\tau^+(p_3) + \tau^-(p_4)$	
004	$Z^0(p_3) + H(p_4)$	[19]
101	$e^+(p_3) + \nu_e(p_4)$	[20, 18]
102	$\mu^+(p_3) + \nu_\mu(p_4)$	
103	$\tau^+(p_3) + \nu_\tau(p_4)$	
-101	$e^-(p_3) + \bar{\nu}_e(p_4)$	
-102	$\mu^-(p_3) + \bar{\nu}_\mu(p_4)$	
-103	$\tau^-(p_3) + \bar{\nu}_\tau(p_4)$	
104	$W^+(p_3) + H(p_4)$	-
-104	$W^-(p_3) + H(p_4)$	
105	$t(p_3) + b(p_4)$ (s-channel)	[21, 22]
106	$t(p_3) + q(p_4)$ (t-channel)	
-105	$\bar{t}(p_3) + b(p_4)$ (s-channel)	
-106	$\bar{t}(p_3) + q(p_4)$ (t-channel)	

Table 1: List of the processes implemented in the `mcsanc-v1.01` integrator with references.

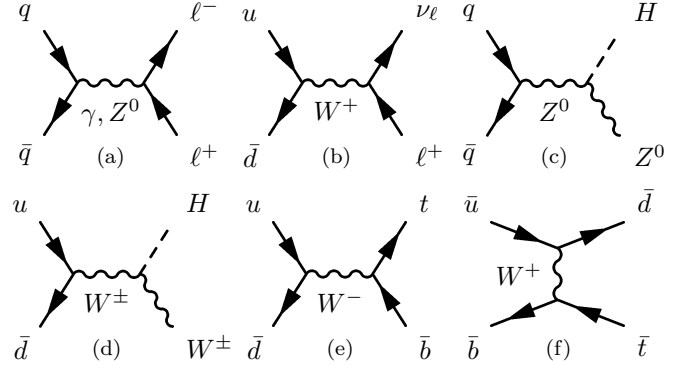


Figure 1: Feynman graphs for tree level Drell-Yan process neutral (a) and charged (b) currents, Higgs and gauge boson production neutral (c) and charged (d) currents, and single top-quark production s-channel (e) and t-channel (f).

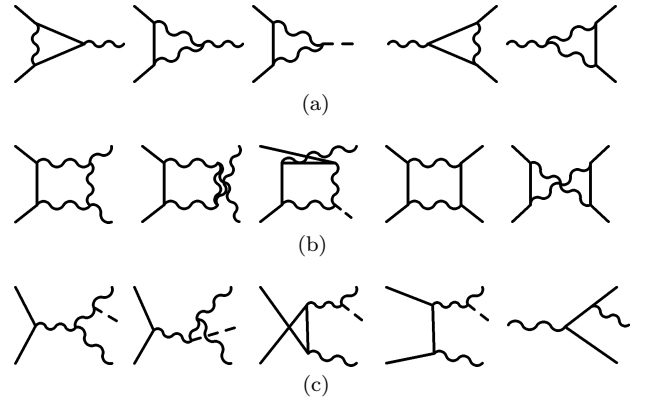


Figure 2: Examples of feynman graphs contributing to EW NLO corrections for Drell-Yan process and associated Higgs and gauge boson production: (a) vertices, (b) boxes and (c) emission.



Figure 3: Examples of feynman graphs contributing to QCD NLO corrections in `mcsanc-v1.01` integrator.

contributions including hard, soft and virtual photon emission. Such initial state mass singularities are well known, for instance, in the process of  $e^+e^-$  annihilation. However, in the case of hadron collisions these logarithms have been already *effectively* taken into account in the parton density functions (PDF). In fact, in the procedure of PDF extraction from experimental data, the QED radiative corrections to the quark line were not systematically subtracted. Therefore current PDFs effectively include not only the QCD evolution but also the QED one. Moreover, it is known that the leading logarithmic behaviours of the QED and QCD DGLAP evolution of the quark density functions are similar (proportional to each other). Consequently one gets an evolution of the PDF with an effective coupling constant

$$\alpha_s^{\text{eff}} \approx \alpha_s + \frac{Q_i^2}{C_F} \alpha, \quad (2)$$

where  $\alpha_s$  is the strong coupling constant,  $\alpha$  is the fine structure constant,  $Q_i$  is the quark charge, and  $C_F$  is the QCD colour factor.

The system supports both  $\overline{\text{MS}}$  and DIS subtraction schemes. A solution described in [23] allows to avoid the double counting of the initial quark mass singularities contained in the results for the corrections to the free quark cross section and the ones contained in the corresponding PDF. The latter should also be taken in the same scheme with the same factorization scale.

For example, the  $\overline{\text{MS}}$  subtraction to the fixed (leading) order in  $\alpha$  is given by:

$$\begin{aligned} \bar{q}(x, M^2) &= q(x, M^2) - \int_x^1 \frac{dz}{z} q\left(\frac{x}{z}, M^2\right) \frac{\alpha}{2\pi} Q_q^2 \\ &\times \left[ \frac{1+z^2}{1-z} \left\{ \ln\left(\frac{M^2}{m_q^2}\right) - 2 \ln(1-z) - 1 \right\} \right]_+ \\ &\equiv q(x, M^2) - \Delta q, \end{aligned}$$

where  $q(x, M^2)$  is the parton density function in the  $\overline{\text{MS}}$  scheme computed using the QED DGLAP evolution.

The differential hadronic cross section for DY processes ( $001 \div 003, \pm 101 \div 103$ ) is given by

$$\begin{aligned} d\sigma^{pp \rightarrow \ell\ell' X} &= \sum_{q_1 q_2} \int_0^1 \int_0^1 dx_1 dx_2 \bar{q}_1(x_1, M^2) \bar{q}_2(x_2, M^2) \\ &\times d\hat{\sigma}^{q_1 q_2 \rightarrow \ell\ell'}, \end{aligned} \quad (3)$$

where  $\bar{q}_1(x_1, M^2), \bar{q}_2(x_2, M^2)$  are the parton density functions of the incoming quarks modified by the subtraction

of the quark mass singularities and  $\sigma^{q_1 q_2 \rightarrow \ell\ell'}$  is the partonic cross section of corresponding hard process. The sum is performed over all possible quark combinations for a given type of process ( $q_1 q_2 = u\bar{d}, u\bar{s}, c\bar{d}, c\bar{s}$  for CC and  $q_1 q_2 = u\bar{u}, d\bar{d}, s\bar{s}, c\bar{c}, b\bar{b}$  for NC). The expressions for other processes are similar.

The effect of applying different EW schemes in the SANC system is discussed in [17]. The SANC system supports  $\alpha(0), G_\mu, \alpha(M_Z)$  (DY NC only) schemes (see comments on EW parameters in Appendix A), of which the  $G_\mu$ -scheme [24] can be preferable since it minimizes EW radiative corrections to the inclusive DY and Higgsstrahlung cross section. In this scheme the weak coupling  $g$  is related to the Fermi constant and the W boson mass by equation

$$g^2 = 4\sqrt{2}G_\mu m_W^2 (1 - \Delta r), \quad (4)$$

where  $\Delta r$  represents all radiative corrections to the muon decay amplitude [25]. Since the vertex term between charged particles and photons is proportional to  $g \sin \theta_W$ , one can introduce an effective electromagnetic coupling constant

$$\alpha_{G_\mu}^{\text{tree}} = \frac{\sqrt{2}G_\mu \sin^2 \theta_W m_W^2}{\pi}, \quad (5)$$

which is evaluated from (4) in a tree-level approximation by setting  $\Delta r = 0$ .

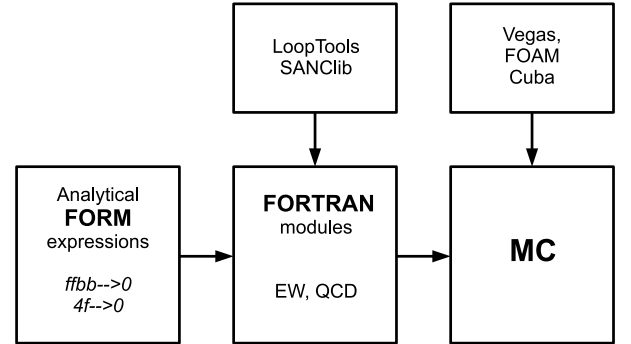


Figure 4: The SANC framework scheme.

The scheme of the SANC framework is shown on the Figure 4. Analytical expressions are obtained for the form-factors and amplitudes of generalized processes  $f f b b \rightarrow 0$  and  $4 f \rightarrow 0$  and stored as the FORM [26] language expressions [11, 19, 27]. The latter are translated to the Fortran modules [12] for specific parton level processes with NLO QCD and EW corrections. The modules are utilising LoopTools [28] and SANClib [29] packages for loop integrals evaluation. To build a Monte-Carlo code one convolutes the partonic cross sections from the modules with the parton density functions and feeds the result as an integrand to any Monte-Carlo algorithm implementation, e.g. FOAM [30] or Cuba [31]. The module's procedures for

partonic cross sections are significantly unified and allow to calculate fully differential hadronic cross sections.

### 3. Numerical validation

The numerical validation was performed using setup given below.

$$\begin{aligned}
\alpha &= 1/137.035999679, & G_F &= 1.16637 \times 10^{-5}, \\
M_W &= 80.399 \text{ GeV}, & M_Z &= 91.1876 \text{ GeV}, \\
M_H &= 120 \text{ GeV}, \\
\Gamma_Z &= 2.4952 \text{ GeV}, & \Gamma_W &= 2.085 \text{ GeV}, \\
V_{ud} &= 0.9738, & V_{us} &= 0.2272, \\
V_{cd} &= 0.2271, & V_{cs} &= 0.9730. \\
V_{ub} &= 0., & V_{cb} &= 0., \\
m_e &= 0.510998910 \text{ MeV}, & m_\mu &= 0.105658367 \text{ GeV}, \\
m_\tau &= 1.77682 \text{ GeV}, \\
m_u &= 0.066 \text{ GeV}, & m_d &= 0.066 \text{ GeV}, \\
m_c &= 1.2 \text{ GeV}, & m_s &= 0.150 \text{ GeV}, \\
m_t &= 172.9 \text{ GeV}, & m_b &= 4.67 \text{ GeV}.
\end{aligned}$$

The electroweak parameters in the  $G_\mu$  scheme were taken from PDG-2011 [32], except for the light quark masses which were taken from [33]. The PDF set was CT10 [34] interfaced via LHAPDF [35] library with the factorization scale equal to renormalization scale and particular for the processes under consideration:  $M_V$  for DY-like single  $V$  production;  $M_{V+H}$  for the processes 004,  $\pm 104$ ;  $m_t$  for the processes  $\pm 105, \pm 106$ .

The phase-space cuts were set to loose values: for the final state particle transverse momenta  $p_T \geq 0.1 \text{ GeV}$ , no cuts for their rapidities and for the neutral current DY, in addition,  $M_{l+l-} \geq 20 \text{ GeV}$ . The numerical results are provided for DY process only for muon case ignoring the effects of recombination. The  $\bar{\omega}$  parameter was set to  $= 10^{-4}$  and the CMS energy to  $\sqrt{s_0} = 14 \text{ TeV}$  if not stated otherwise.

At NLO level several hard sub-processes contribute to a given process. In general, it consists of several parts: LO – leading order, *virt* – virtual, *real* brems(glue)-strahlung and *subt* – subtraction; *real*, in turn, is subdivided into *soft* and *hard* contributions. All contributions are enumerated with **id**=0–6:

- id0**: LO,  $2 \rightarrow 2$ , tree-level,  $q\bar{q}'$  NC or CC sub-processes.
- id1**: *subt* term, responsible for the subtraction of the initial quark mass ( $m_q$ ) singularities for  $q\bar{q}'$  sub-processes, computed in a given subtraction scheme ( $\overline{\text{MS}}$  or DIS). It depends on  $\ln(m_q)$ .
- id2**: *virt* represents only the NLO EW parts, stands for pure EW one-loop virtual contributions. It depends on  $m_q$  and may depend on an infrared regulator (e.g. on an infinitesimal photon mass). It is not present for NLO QCD contributions, where it is added to the soft contribution (see next item). For DY NC NLO EW process it contains all virtual contributions, both EW and QED.

$pp \rightarrow$	$Z^0(\mu^+\mu^-)$	$W^+(\mu^+\nu_\mu)$	$W^-(\mu^-\bar{\nu}_\mu)$
LO	3338(1)	10696(1)	7981(1)
LO MCFM	3338(1)	10696(1)	7981(1)
NLO QCD	3388(2)	12263(4)	9045(4)
NLO MCFM	3382(1)	12260(1)	9041(5)
NLO EW	3345(1)	10564(1)	7861(1)
$\delta_{QCD}, \%$	1.49(3)	14.66(1)	13.35(3)
$\delta_{EW}, \%$	0.22(1)	-1.23(1)	-1.49(1)

Table 2: NC and CC DY processes, i.e. for **pid** = 002,  $\pm 102$ . LO, NLO EW, NLO QCD cross sections are given in picobarns and compared with corresponding values obtained with the program MCFM. The correction factors  $\delta$  are shown in %.

$pp \rightarrow$	$Z^0 + H$	$W^+ + H$	$W^- + H$
LO	0.8291(1)	0.9277(1)	0.5883(1)
LO MCFM	0.8292(1)	0.9280(2)	0.5885(1)
NLO QCD	0.9685(3)	1.0897(3)	0.6866(3)
NLO MCFM	0.9686(1)	1.0901(2)	0.6870(1)
NLO EW	0.7877(1)	0.8672(2)	0.5508(1)
$\delta_{QCD}, \%$	16.81(3)	17.47(3)	16.72(5)
$\delta_{EW}, \%$	-5.00(2)	-6.52(2)	-6.38(3)

Table 3: The same is in Table 2 but for processes of  $HZ(W^\pm)$  production, i.e. **pid**= 004,  $\pm 104$ .

- id3**: For all processes, except DY NC, this stands for the sum of *virt* and *real soft* (QED/QCD) contributions, therefore it does not depend on the infrared regulator but depends on  $m_q$  and on the soft-hard separator  $\bar{\omega}$ . For DY NC NLO EW processes it is just the *real soft* QED contribution that depends on the infrared regulator, on  $m_q$  and on the soft-hard separator  $\bar{\omega}$ .
- id4**: For all processes this is just the *real hard* (QED/QCD) contribution that depends on  $m_q$  and on  $\bar{\omega}$ .
- id5**: *subt* term is responsible for the subtraction of the initial quark mass singularities for  $q\bar{q}(q\bar{q}')$  sub-processes (also computed in  $\overline{\text{MS}}$  or DIS schemes). It contains logarithmic singularities in  $m_q$ .
- id6**: The gluon-induced sub-process – an analog of **id4** for  $g\bar{g}(g\bar{g}')$  sub-processes. They also contain logarithmic mass singularities which cancel those from **id5**.

The quark mass is used to regularize the collinear divergences, the soft-hard separator is a remainder of infrared divergences. The sum of contributions with **id3** and **id4** is independent of  $\bar{\omega}$ . The sums **id1**+**id2**+**id3**+**id4** and **id5**+**id6** are separately independent of  $m_q$ . Therefore, the entire NLO sub-process is independent of both unphysical parameters  $\bar{\omega}$  and  $m_q$ .

Tables 2-4 contain results for integrated LO and NLO EW and QCD cross sections obtained with the **mcsanc-v1.01** integrator. The LO and NLO QCD values are in

$pp \rightarrow$	$t + b$ (s-channel)	$\bar{t} + b$ (s-channel)
LO	5.134(1)	3.205(1)
LO MCFM	5.133(1)	3.203(1)
NLO QCD	6.921(2)	4.313(2)
NLO MCFM	6.923(2)	4.309(1)
NLO EW	5.022(1)	3.140(1)
$\delta_{QCD}, \%$	34.79(5)	34.56(8)
$\delta_{EW}, \%$	-2.18(1)	-2.02(2)
$pp \rightarrow$	$t + q$ (t-channel)	$\bar{t} + q$ (t-channel)
LO	158.73(2)	95.18(2)
LO MCFM	158.69(7)	95.27(4)
NLO QCD	152.13(9)	90.44(7)
NLO MCFM	152.07(14)	90.50(8)
NLO EW	164.44(5)	98.65(4)
$\delta_{QCD}, \%$	-4.17(6)	-4.08(8)
$\delta_{EW}, \%$	3.59(3)	3.66(5)

Table 4: The same is in Table 2 but for single top production, s- and t-channels, i.e. for  $\text{pid} = \pm 105, \pm 106$ .

agreement with the MCFM [5] program within statistical error. A detailed comparison of differential neutral current Drell–Yan cross section is shown on Figures 5 and 6 for dilepton invariant mass and lepton transverse momentum distributions correspondingly. The lower plots on these figures show good agreement between NLO QCD correction factors obtained with `mcsanc`-v1.01 and MCFM.

Plots on Figures 7, 8 show separate EW and QCD contributions to the differential NC DY cross section and their sum. The electroweak radiation produce high corrections around the Z resonance peak for the dilepton invariant mass distribution, while the QCD corrections are flatter.

## 4. Summary

The presented `mcsanc` integrator is a new Monte-Carlo tool for evaluating higher order (NLO) EW and QCD cross sections. The integrator is based on the SANC framework modules and calculates integrated and differential cross sections for Drell–Yan processes, associated Higgs and gauge boson production and single-top quark production. The code was thoroughly cross checked against another tools to provide consistent results. `mcsanc` uses advantage of multicore implementation of the Cuba Monte-Carlo integration library and supports simple histogramming setup.

## 5. Acknowledgements

This work was supported in part by the RFBR grants 12-02-91526-CERN\_a and by the Dynasty Foundation.

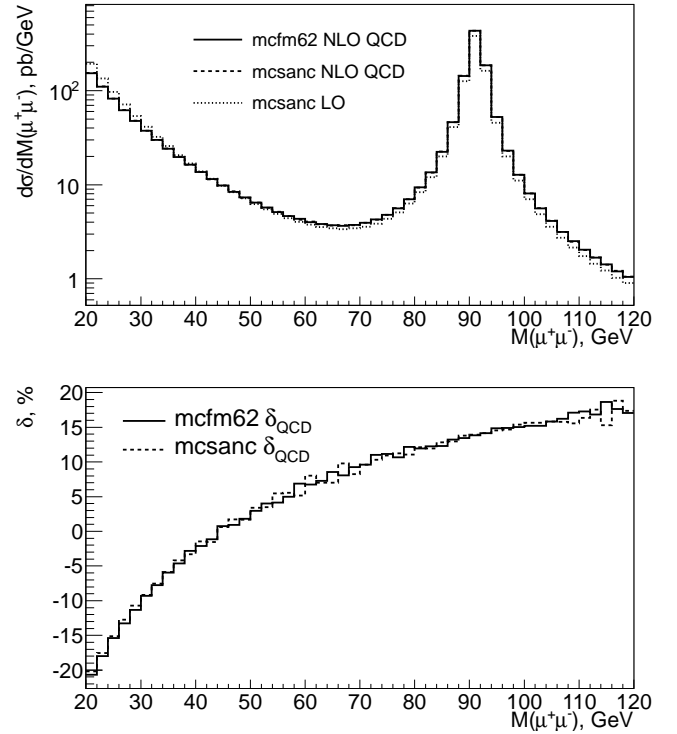


Figure 5: Comparison of differential cross sections and correction factors  $\delta(\text{QCD})$  for neutral current Drell–Yan  $pp \rightarrow \mu^+ \mu^-$  process in dilepton invariant mass distribution.

## Appendix A. mcsanc program

### Appendix A.1. Installation

The LHAPDF [35] is required to be installed before starting the installation. After downloading and unpacking the tarball with `mcsanc` from <http://sanc.jinr.ru> perform the following steps.

```
cd mcsanc_vXX
./configure [--with-LHAPDF=/custom/LHAPDF/path]
make
```

If succeeded the executable will be created in `./src` directory. The program is launched with a command from `./share`:

```
cd ./share
../src/mcsanc [custom-input.cfg]
```

Upon completion an output file `mcsanc-[run_tag]-output.txt` with final results, run parameters and histograms will be created in the current directory.

### Appendix A.2. Configuration

The `mcsanc` program reads to configuration files upon start: `input.cfg` and `ewparam.cfg`. The first file, `input.cfg`, contains general steering parameters for a run, VEGAS parameters, kinematic cuts and histogram parameters organized in Fortran namelists.

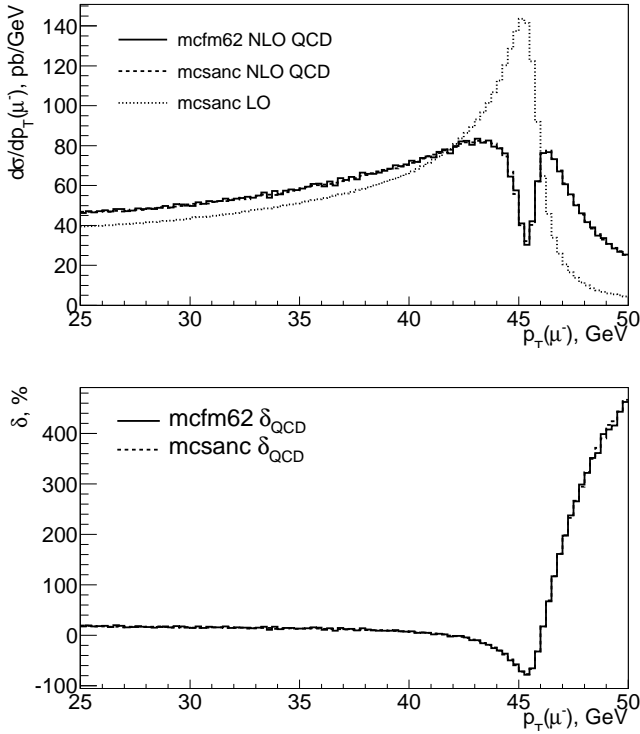


Figure 6: Comparison of differential cross sections and correction factors  $\delta(\text{QCD})$  for neutral current Drell-Yan  $pp \rightarrow \mu^+\mu^-$  process muon transverse momentum distributions.

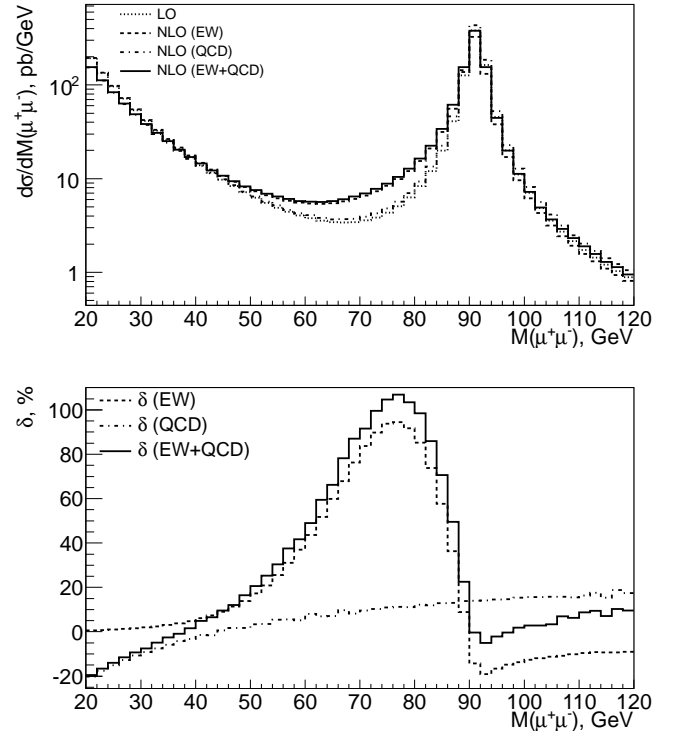


Figure 7: A comparative representation of EW and QCD contributions to NLO corrections and their sum for NC DY process  $pp \rightarrow \mu^+\mu^-$  for the dilepton invariant mass distribution.

#### Appendix A.2.1. Process namelist

**processId** defines a process to calculate (for available processes see Table 1)(**integer**).

**run\_tag** is an arbitrary string value (**character\*256**).

**sqs0** sets the beam energy at CMS frame (**double precision**).

**beams(2)** defines the incoming beams. So far only proton-proton beams are supported, which corresponds to **beams** = 1,1 (**integer**).

**PDFSet** allows to set the parton density functions connected via LHAPDF (**character\*256**).

**PDFMember** selects a member of PDF set. Usually 0 is used, which corresponds to central value (**integer**).

**ifew(5)** flags controlling electroweak components of the NLO EW computations. See below. (**integer**).

**iqed** =

- 0: disables QED corrections
- 1: with full QED corrections
- 2: only initial state QED radiation (ISR)
- 3: initial-final QED radiation interference term (IFI)
- 4: only final state QED radiation (FSR)

5: sum of initial and final state radiation contributions [IFI+FSR] (only for pid=001 ÷ 003, ±101 ÷ 103)

6: sum of initial state and initial-final QED interference terms [ISR+IFI] (only for pid=001 ÷ 003)

**iew** = 0/1 corresponds to disabled/enabled weak corrections.

**iborn** 0 or 1 selects respectively LO or NLO level of calculations.

**ifgg** = choice of calculations for photonic vacuum polarization  $\mathcal{F}_{\gamma\gamma}$ :

- 1: 0
- 0: 1
- 1:  $1 + \mathcal{F}_{\gamma\gamma}(\text{NLO})$
- 2:  $1/[1 - \mathcal{F}_{\gamma\gamma}(\text{NLO})]$

**irun** = 0/1 corresponds to fixed/running gauge boson width

**iflqcd** controls if NLO QCD is calculated (**integer**).

**imsb** allows to select a subtraction scheme: 0/1/2 = none/MSbar/DIS (**integer**).

**irecomb** electron recombination option: 0/1 = off/on (**integer**).

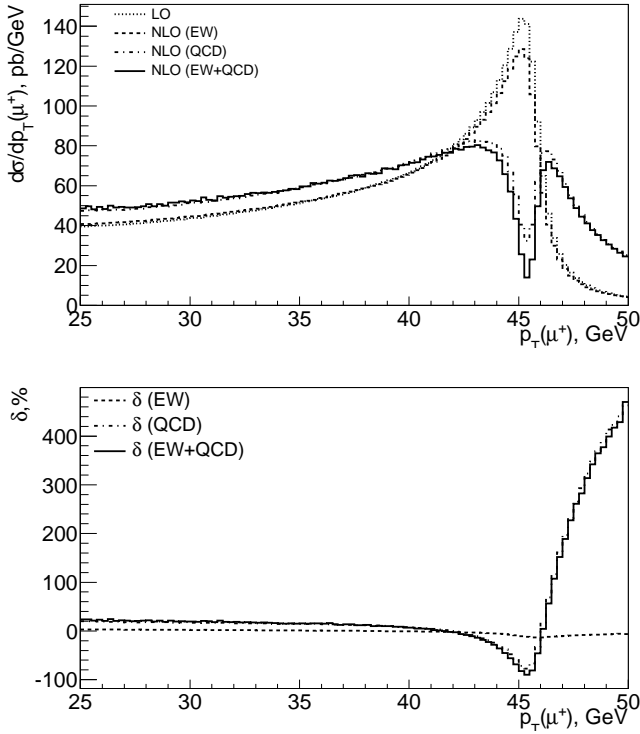


Figure 8: A comparative representation of EW and QCD contributions to NLO corrections and their sum for NC DY process  $pp \rightarrow \mu^+ \mu^-$  for the lepton transverse momentum distribution.

#### Appendix A.2.2. VegasPar namelist

VegasPar regulates VEGAS parameters:

- relAcc** relative accuracy limit on the calculated cross section (**double precision**)
- absAcc** absolute accuracy limit on the cross section (**double precision**)
- nstart** number of integrand evaluations performed at first iteration (**integer**)
- nincrease** increment of integrand evaluations per iteration (**integer**)
- nExplore** number of evaluations for grid exploration (**integer**)
- maxEval** maximum number of evaluations (**integer**)
- seed** random generator seed (**integer**)
- flags** Cuba specific flags. See Cuba manual for more information [31] (**integer**)

Different contributions to NLO cross sections (real, virtual) can differ from each other by orders of magnitude. The combination of relative and absolute accuracy limits gives a suitable way to control accuracy of total cross section without need to limit each contribution. For example,

the goal is 0.1% relative accuracy on total cross section. The user can set this value to the **relAcc** option with an allowance for summing of the contributions. The absolute error limit can then be calculated multiplying this value by the largest estimated contribution. This will cut off unnecessary long calculations for smaller contributions.

#### Appendix A.2.3. KinCuts namelist

This configuration section contains typical kinematic cuts for fiducial cross section calculation. Besides original cuts, the user is free to implement his own in the **src/kin\_cuts.f**. The cut values are set under corresponding name in the table in **input.cfg**

```
&KinCuts
  cutName      = 'm34', 'mtr', 'pt3', 'eta3', ...
  cutFlag      = 1,    0,    1,    1,    ...
  cutLow       = 66d0, 66d0, 20d0, -2.5d0, ...
  cutUp       = 116d0, 116d0, 7d3,  2.5d0, ...
/
```

The **cutName** fields are fixed, **cutFlag** - 0/1 on/off cuts. By default seven kinematic cuts are foreseen. They are: invariant **m34** and transversal **mtr** masses, transversal momenta **pt3**, **pt4**, rapidities **eta3**, **eta4** of the final particles and **dR** parameter to calculate recombined lepton momentum.

#### Appendix A.2.4. Histograms with equidistant bins

Namelist **FixedBinHist** allows to control histograms with fixed step. The histogram parameters are defined in a table: under the histogram name, the user can set printing flag, min and max histogram values and a step. The binary printing flag controls if histogram is printed in the output (first bit) and if it's normalized to the bin width (second bit). For example to print unnormalized histograms set the flag to 1, to print normalized to 3.

```
&FixedBinHist
  fbh_name     = 'm34', 'mtr', 'pt34', 'pt3', 'et3', ...
  fbh_flag     = 3,    3,    0,    3,    3,    ...
  fbh_low      = 66d0, 66d0, 20d0, 20d0, -2.5d0, ...
  fbh_up       = 116d0, 116d0, 58d0, 58d0, 2.5d0, ...
  fbh_step     = 2d0,  2d0,  1d0,  1d0,  0.125d0, ...
/
```

The most common parameters like invariant **m34** and transversal **mtr** masses, transversal momenta **pt3**, **pt4** rapidities **eta3**, **eta4** of the final particles and transversal momenta **pt34** of intermediate boson are included by default.

Any user defined histograms can be implemented in the **src/kin\_cuts.f** file. There the histogram names have no technical meaning, the requirement is that the order of histograms in the input file must correspond to the histogram array **hist\_val** and the **nhist** variable set to the number of requested histograms.

### Appendix A.2.5. Histograms with variable bins

Variable bin histograms are defined in namelist **VarBinHist**. The format is different from **FixedBinHist**. The user have to set total number of variable step histograms with **nvbh** parameter. Then follows definition of corresponding to  $i$ 'th histogram name (**vbh\_name(i)**), printing flag (**vbh\_flag(i)**), number of bins (**vbh\_nbins(i)**) and array for the bin edges (**vbh\_bins(i,1:[nbins+1])**) as a space separated string of double precision numbers. It is important that the variable bin histograms are available only with **gcc-v4.5.0** and higher.

```
&VarBinHist
  nvbh          = 7,

  vbh_name(1) = 'm34',
  vbh_flag(1) = 3,
  vbh_nbins(1) = 6,
  vbh_bins(1,1:7) = 50d0 55d0 60d0 70d0 100d0 200d0,

  vbh_name(2) = 'mtr',
  vbh_flag(2) = 0,
  vbh_nbins(2) = 6,
  vbh_bins(2,1:7) = 50d0 55d0 60d0 70d0 100d0 200d0,

  vbh_name(3) = 'pt34',
  vbh_flag(3) = 3,
  vbh_nbins(3) = 5,
  vbh_bins(3,1:10) = 25d0 30d0 50d0 70d0 90d0 110d0,

  ...
/
```

Some common kinematic variables are included in variable bin histograms by default.

### Appendix A.3. Electroweak parameters

Electroweak parameters are set in **ewparams.cfg** configuration file. It contains **&EWParams** name list with the following fields.

**gfscheme** flag selects electroweak scheme in which the calculation is performed (**integer**). The possible values are 0: $\alpha(0)$ -scheme, 2: $G_\mu$ -scheme, 4: $\alpha(M_Z)$ -scheme (only for pid=001,002,003).

**fscale** is the factorization scale (**double precision**). When equals -1, the value appropriate for requested process is set (e.g. final lepton invariant mass for DY process). Otherwise the given value is used.

**rscale** - renormalization scale defined with the same rules as **fscale** (**double precision**).

**ome** is the parameter separating contributions from soft and hard photon radiation (**double precision**).

**alpha, gf, alphas, conhc** - a list of constants and coefficients:  $\alpha_{EM}$ ,  $G_\mu$ ,  $\alpha_S$ , conversion constant (**double precision**)

**mw, mz, mh** boson masses W, Z, Higgs (**double precision**)

**wz, ww, wh, wtp** widths for bosons W, Z, Higgs and the top quark (**double precision**)

**Vqq** CKM matrix (**double precision**)

**men, mel, mmn, mmo, mtn, mta** leptonic masses  $\nu_e, e, \nu_\mu, \mu, \nu_\tau, \tau$  (**double precision**)

**mdn, mup, mst, mch, mbt, mtp** quark masses  $u, d, s, c, b, t$  (**double precision**)

**mfact** quark mass factor(**double precision**). The total NLO EW cross sections should be independent on this parameter as the quark masses should cancel.

**rmf1** is a 12 element array of fermion masses for technical purposes (**double precision**)

Vegas grids have to be generated from scratch if these parameters are changed.

### Appendix A.4. Persistency

Cuba library [31] allows to save the VEGAS grid for further restoration. The integration stops when requested accuracy is reached. The last version of the grid and histograms state are saved in **\*.vgrid** and **\*.hist** files. If the user desires to improve precision he can set the new limits in **input.cfg** and restart the program in the directory with saved grids. Care should be taken that all other configurations (PDF, electroweak parameters) are remained the same. If the user wishes to change the histograms he can use old grids, but remove **\*.hist** files and fill the histograms from scratch. The histogram errors will correspond to less precision than the total cross section.

The grid exploration stage is omitted if grid state file is found.

### Appendix A.5. Output

The main output of the program will be written to **mcsanc-[run\_tag]-output.txt** file. The file contains final table with cross sections from the components and the summed total cross section. After the table follows the CPU usage, and a list of input parameters, followed by a list of cuts applied in the process of integration. The remaining of the output file is a section containing Histograms listing. Each histogram is output separately in a text file for plotting convenience. The file name format is **[run\_tag]\_[hist\_name]-XXX**, where XXX stands for **born**, **tota** or **delt** for LO, NLO and  $\delta\%$  histograms.

## Appendix B. Multiprocess calculations

The Cuba library [31], used as a Monte-Carlo integrating tool in the **mcsanc** program, supports multiprocessing. Having a multicore CPU the user can request the program



to run on several cores by specifying CUBACORES environment variable.

Due to the features of inter-process communications, the efficiency of multiprocessing is not always optimal. Figure B.9 shows NLO EW cross section calculation time depending on the number of CPU cores active. The test was run on a dual-processor Intel® Xeon® machine with 12 real (24 virtual) cores with Linux operating system.

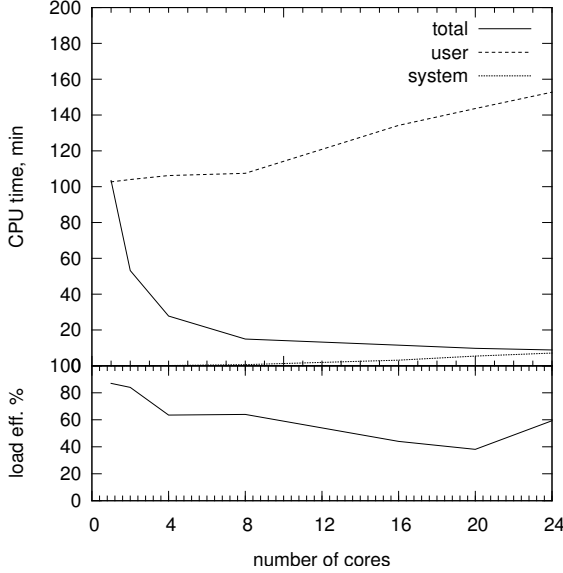


Figure B.9: CPU usage and load efficiency for `mcsanc` program depending on the number of processor cores.

The upper plot summarizes multicore CPU productivity: “total” is the wall clock time passed during the run; “user” is the CPU time consumed by the program (roughly equals to wall clock time multiplied by the number of cores in case of 100% efficiency); “system” is the time spent by the operating system on the multiprocessing service. One can see that the multiprocessing is efficient with number of cores up to 8, after which the total run time does not significantly decrease and the CPU time (“user”) grows. It is also clear from the lower plot that the average CPU load efficiency drops below 50% with more than 8 cores active.

## References

- [1] S. Catani and M. Grazzini, *Phys.Rev.Lett.* **98** (2007) 222002, [hep-ph/0703012](#).
- [2] S. Catani, L. Cieri, G. Ferrera, D. de Florian, and M. Grazzini, *Phys.Rev.Lett.* **103** (2009) 082001, [0903.2120](#).
- [3] Y. Li and F. Petriello, *Phys.Rev.* **D86** (2012) 094034, [1208.5967](#).
- [4] W. Giele, E. N. Glover, and D. A. Kosower, *Nucl.Phys.* **B403** (1993) 633–670, [hep-ph/9302225](#).
- [5] J. M. Campbell and R. Ellis, *Nucl.Phys.Proc.Suppl.* **205-206** (2010) 10–15, [1007.3492](#).
- [6] S. Brensing, S. Dittmaier, . Kramer, Michael, and A. Muck, *Phys.Rev.* **D77** (2008) 073006, [0710.3309](#).

- [7] U. Baur, O. Brein, W. Hollik, C. Schappacher, and D. Wackeroth, *Phys.Rev.* **D65** (2002) 033007, [hep-ph/0108274](#).
- [8] C. Carloni Calame, G. Montagna, O. Nicrosini, and A. Vicini, *JHEP* **0710** (2007) 109, [0710.1722](#).
- [9] C. Carloni Calame, G. Montagna, O. Nicrosini, and A. Vicini, *JHEP* **0612** (2006) 016, [hep-ph/0609170](#).
- [10] D. Bardin, S. Bondarenko, P. Christova, L. Kalinovskaya, L. Romyantsev, *et al.*, *JETP Lett.* **96** (2012) 285–289, [1207.4400](#).
- [11] A. Andonov *et al.*, *Comput. Phys. Commun.* **174** (2006) 481–517, [hep-ph/0411186](#).
- [12] A. Andonov, A. Arbuzov, D. Bardin, S. Bondarenko, P. Christova, *et al.*, *Comput.Phys.Comm.* **181** (2010) 305–312, [arXiv:0812.4207](#).
- [13] D. Y. Bardin and G. Passarino, Oxford, UK: Clarendon (1999) 685 p.
- [14] M. Greco, G. Pancheri-Srivastava, and Y. Srivastava, *Nucl.Phys.* **B171** (1980) 118.
- [15] M. Bohm and W. Hollik, *Nucl.Phys.* **B204** (1982) 45.
- [16] A. Denner, *Fortsch.Phys.* **41** (1993) 307–420, [0709.1075](#).
- [17] A. Arbuzov, D. Bardin, S. Bondarenko, P. Christova, L. Kalinovskaya, *et al.*, *Eur.Phys.J.* **C54** (2008) 451–460, [arXiv:0711.0625](#).
- [18] A. Andonov, A. Arbuzov, S. Bondarenko, P. Christova, V. Kolesnikov, *et al.*, *Phys.Atom.Nucl.* **73** (2010) 1761–1769, [0901.2785](#).
- [19] D. Bardin, S. Bondarenko, L. Kalinovskaya, G. Nanava, L. Romyantsev, *et al.*, *Comput.Phys.Comm.* **177** (2007) 738–756, [hep-ph/0506120](#).
- [20] A. Arbuzov, D. Bardin, S. Bondarenko, P. Christova, L. Kalinovskaya, *et al.*, *Eur.Phys.J.* **C46** (2006) 407–412, [hep-ph/0506110](#).
- [21] D. Bardin, S. Bondarenko, L. Kalinovskaya, V. Kolesnikov, and W. von Schlippe, *Eur.Phys.J.* **C71** (2011) 1533, [1008.1859](#).
- [22] D. Bardin, S. Bondarenko, P. Christova, L. Kalinovskaya, V. Kolesnikov, *et al.*, *Pepan Lett.* **9** (2012) 770–787, [1110.3622](#).
- [23] K.-P. Diener, S. Dittmaier, and W. Hollik, *Phys.Rev.* **D72** (2005) 093002, [hep-ph/0509084](#).
- [24] G. Degrandi, P. Gambino, and A. Sirlin, *Phys. Lett.* **B394** (1997) 188–194, [hep-ph/9611363](#).
- [25] A. Sirlin, *Phys.Rev.* **D22** (1980) 971–981.
- [26] J. A. M. Vermaseren, [math-ph/0010025](#).
- [27] A. Arbuzov, D. Bardin, S. Bondarenko, P. Christova, L. Kalinovskaya, *et al.*, *Eur.Phys.J.* **C51** (2007) 585–591, [hep-ph/0703043](#).
- [28] T. Hahn and M. Perez-Victoria, *Comput. Phys. Commun.* **118** (1999) 153–165, [hep-ph/9807565](#).
- [29] D. Bardin, L. Kalinovskaya, V. Kolesnikov, and W. von Schlippe, *Phys.Atom.Nucl.* **73** (2010) 2048–2063, [0912.3893](#).
- [30] S. Jadach and P. Sawicki, *Comput. Phys. Commun.* **177** (2007) 441–458, [physics/0506084](#).
- [31] T. Hahn, *Comput.Phys.Comm.* **168** (2005) 78–95, [hep-ph/0404043](#).
- [32] Particle Data Group Collaboration, K. Nakamura *et al.*, *J.Phys.* **G37** (2010) 075021.
- [33] S. Dittmaier and M. Huber, *JHEP* **01** (2010) 060, [0911.2329](#).
- [34] M. Guzzi, P. Nadolsky, E. Berger, H.-L. Lai, F. Olness, *et al.*, [1101.0561](#).
- [35] M. R. Whalley, D. Bourilkov, and R. C. Group, [hep-ph/0508110](#).